Synthesis and Structure Determination of (hfac)Ag(SEt_2), Pd(hfac-*C*)(hfac-*O,O*)(SEt_2), and [(hfac)Ag]$_4$(SEt_2): Ligand Exchange Reactions Relevant to Aerosol-Assisted Chemical Vapor Deposition (AACVD) of $Ag_{1-x}Pd_x$ Films

Chongying Xu,[†] Mark J. Hampden-Smith,*[,†] Toivo T. Kodas,*[,‡] and Eileen N. Duesler[†]

Departments of Chemistry and Chemical Engineering, University of New Mexico, Albuquerque, New Mexico 87131

Arnold L. Rheingold and Glenn Yap

Department of Chemistry, University of Delaware, Newark, Delaware 19716

Received February 24, 1995[⊗]

This paper describes the solution chemistry of the species (hfac)Ag(SEt_2) and Pd(hfac)$_2$ which have been used as metal−organic precursors for the aerosol-assisted (AA) chemical vapor deposition (CVD) of $Ag_{1-x}Pd_x$ alloy films. The reaction between (hfac)Ag(SEt_2) and Pd(hfac)$_2$ was investigated in toluene solution and found to result in a reaction with formation of the species Pd(hfac-*C*)(hfac-*O,O*)(SEt_2) and [(hfac)Ag]$_4$(SEt_2). These two species were characterized in solution by NMR spectroscopy and in the solid state by FTIR, elemental analysis, and single-crystal X-ray diffraction. The solid state structure of Pd(hfac-*C*)(hfac-*O,O*)(SEt_2) confirmed the monomeric square planar four-coordinate structure of this molecule with two different hfac bonding modes. Crystal data: empirical formula $C_{14}H_{12}PdF_{12}O_4S$: crystal system monoclinic; space group $P2_1/n$; unit cell dimensions a = 9.0273(9) (2), b = 26.248(3), c = 9.763(8) Å; β = 103.042(2)°; Z = 4. The species [(hfac)Ag]$_4$(SEt_2), comprised "(hfacAg)$_4$" tetramers connected by bridging SEt_2 groups to form an infinite polymer. This structure is remarkable for the presence of unusual unsupported μ-SEt_2 and μ_4-hfac ligand binding modes. Crystal data: empirical formula $C_{24}H_{14}Ag_4F_{24}O_8S$; crystal system monoclinic; space group $C2/c$; unit cell dimensions a = 24.776(2), b = 9.5179-(8), c = 19.940(3) Å; β = 126.724(8)°; Z = 4. The observation of this unusual coordination mode for μ-SEt_2 prompted us to structurally characterize (hfac)Ag(SEt_2) in the solid state by single-crystal X-ray diffraction. Crystal data: empirical formula $C_9H_{11}AgF_6O_2S$; crystal system hexagonal; space group $P6_122$; unit cell dimensions a = 10.853(4), c = 18.850(1) Å; Z = 6. This compound is monomeric in the solid state with a unidentate SEt_2 ligand. The observation of this ligand exchange reaction between (hfac)Ag(SEt_2) and Pd(hfac)$_2$ in a 1:1 mole ratio with formation of the species Pd(hfac-*C*)(hfac-*O,O*)(SEt_2) and [(hfac)Ag]$_4$(SEt_2) leads to the following balanced equation: 4(hfac)Ag(SEt_2) + 3Pd(hfac)$_2$ ⇌ 3Pd(hfac-*C*)(hfac-*O,O*)(SEt_2) + [(hfac)Ag]$_4$(SEt_2). When this reaction was repeated by mixing the reagents in the correct mole ratios as defined in the preceding equation, the product Pd(hfac-*C*)(hfac-*O,O*)(SEt_2) was obtained in only 45−50% yield in solution as determined by ^{1}H NMR integration and unreacted Pd(hfac)$_2$ was observed, consistent with the presence of an equilibrium between all the species involved. In order to prevent this ligand exchange reaction in solutions containing both Ag(I) and Pd(II) compounds required for AACVD of $Ag_{1-x}Pd_x$ alloys, it is reasonable to use Pd(hfac-*C*)(hfac-*O,O*)(SEt_2) as a Pd source. It is shown that Pd(hfac-*C*)(hfac-*O,O*)(SEt_2) and (hfac)Ag(SEt_2) do not undergo ligand exchange (or any other reaction) in toluene solution, and so represent a suitable source for the deposition of $Ag_{1-x}Pd_x$ alloys by AACVD.

Introduction

Chemical vapor deposition (CVD) is a process in which a volatile metal-containing compound is transported to a heated substrate under controlled conditions where it reacts to form a thin film of the desired material.[1] One of the largest problems associated with CVD of metal films is the low volatility of many metal-containing compounds.[2] Precursors which are gaseous at room temperature such as WF_6 are most desirable because their delivery rates and partial pressures can be controlled using mass flow controllers.[3,4] However, most metal-containing compounds are either liquids or solids at room temperature with vapor pressures that rarely exceed 1 Torr, even when they are heated. As a result, the deposition rate is often limited by the rate of transport of the metal-containing compound from its container to the deposition zone. In addition, the heated precursor often decomposes slowly, leading to the formation of volatile byproducts which add to the mass flow and partial pressure in the reactor, thereby changing the deposition rate in an uncontrolled manner.

In order to alleviate these problems, a number of alternative precursor transport methods are being developed which generally involve transport of a precursor solution to the deposition apparatus.[5] Examples of this method include liquid delivery,[6−8] supercritical fluid transport (SCT) CVD,[9] spray metal−organic (MO) CVD,[10−17] and aerosol-assisted (AA) CVD.[18−29] We have

* Authors to whom correspondence should be addressed.
[†] Department of Chemistry.
[‡] Department of Chemical Engineering.
[⊗] Abstract published in *Advance ACS Abstracts,* September 1, 1995.
(1) Kodas, T. T., Hampden-Smith, M. J., Eds. *The Chemistry of Metal CVD*; VCH: Weinheim, 1994.
(2) Jaraith, R.; Jain, A.; Tolles, R. D.; Hampden-Smith, M. J.; Kodas, T. T. In *The Chemistry of Metal CVD*; Kodas, T. T., Hampden-Smith, M. J., Eds.; VCH: Weinheim, 1994; Chapter 1.
(3) Zinn, A. *The Chemistry of Metal CVD*; VCH: Weinheim, 1994; Chapter 3.
(4) McConica, C. M.; Krishnamani, K. *J. Electrochem. Soc.* **1986**, *133*, 2542.

0020-1669/95/1334-4767$09.00/0

chosen to explore AACVD due to the high level of control and wide range of conditions under which this delivery method can be operated. In addition to improving the deposition rate,[29] AACVD also has the added advantages that it broadens the range of compounds that can be used for CVD by facilitating transport of compounds with relatively low vapor pressures and low thermal stabilities from which it would otherwise be impossible to carry out film deposition. These aspects were recently demonstrated for the CVD of silver films from (hfac)-$Ag(SEt_2)$, where hfac = 1,1,1,5,5,5-hexafluoroacetylacetonate.[28] A further advantage of these precursor delivery techniques is the potential simplicity of the deposition of films with more complex stoichiometries in which control over composition is crucial to the properties of the film. In traditional precursor delivery systems, it is necessary to control the partial pressures of the precursors using heated mass flow controllers, which is extremely difficult for low volatility metal-containing compounds.

We are currently studying the AACVD of binary and ternary alloy films prepared from the elements Ag, Pd, and Cu and have demonstrated that binary alloy films can be deposited at various compositions from solutions that contain different mole ratios of Ag(I), Pd(II), or Cu(II) precursors.[30] The deposition of binary films from a solution adds an additional design criterion to those required for the synthesis of precursors for CVD: the precursors should not react in the precursor solution prior to delivery to the substrate, because such a reaction may lead to formation of involatile species.

In this paper, we present the results of a study which shows that the Ag(I) and Pd(II) compounds used as precursors for the AACVD of $Ag_{(1-x)}Pd_x$ films undergo a ligand exchange reaction in toluene solution to form larger aggregates, which may be detrimental to AACVD of these materials. The results of this study have led to a strategy to redesign the precursors to avoid this ligand exchange reaction and provide better control over the deposition process. The synthesis and characterization of the compounds (hfac)$Ag(SEt_2)$, $[(hfac)Ag]_4(SEt_2)$, and $Pd(hfac)_2$-(SEt_2) are described.

Experimental Section

All manipulations were carried out under an atmosphere of dry dinitrogen using standard Schlenk techniques.[31] All hydrocarbon and ethereal solvents were dried and distilled from sodium benzophenone ketyl and stored over 4 Å molecular sieves. Silver(I) oxide, 1,1,1,5,5,5-hexafluoroacetylacetone (hfacH), $Pd(hfac)_2$, and ethyl sulfide were purchased from Aldrich Chemical Co. and used without further purification. The compound (hfac)$Ag(SEt_2)$ was prepared according to the literature procedure.[32]

Elemental analyses (EA) were performed by Ms. R. Ju at the Department of Chemistry, University of New Mexico. Nuclear magnetic resonance spectra were recorded on a Bruker AC-250P NMR spectrometer by using the protio impurities of the deuterated solvents as reference for the ^1H NMR and the ^{13}C resonance of the solvents as reference for $^{13}C\{^1H\}$ NMR spectroscopy. Infrared data were recorded on a Perkin-Elmer model 1620 FTIR spectrophotometer. Single-crystal X-ray diffraction data were collected on a Nicolet R3m/v diffractometer. The structures were solved by direct methods using SHELXTL Plus and refined by the full-matrix least-squares method. Melting point data were obtained on a Thomas-Hoover capillary melting point apparatus.

Syntheses. A typical experimental procedure is given for each compound, followed by the relevant characterization data.

(a) Reaction between (hfac)$Ag(SEt_2)$ and $Pd(hfac)_2$. To a mixture of (hfac)$Ag(SEt_2)$ (0.100 g, 0.21 mmol) and $Pd(hfac)_2$ (0.110 g, 0.21 mmol, 1.00 equiv) was added by a syringe 5 mL of dry toluene at room temperature. The resulting mixture was stirred for 5 min, and the solids dissolved to give an orange solution. The whole solution was cooled to −30 °C overnight, and yellow cube-shape crystals were formed and were isolated by filtration. The mother liquor was concentrated by partial removal of the solvent *in vacuo* and cooled to −30 °C for 24 h, and a second crop of yellow crystals was isolated. This procedure was repeated several times until the mother liquor was pale yellow. The yellow product was characterized as Pd(hfac-*C*)-(hfac-*O,O*)(SEt_2) by NMR, EA, and single-crystal X-ray diffraction. Removal of all volatile components from the rest of the mother liquor gave a pale yellow-white powder, which was dissolved in 0.5 mL of ether followed by slow addition of 3 mL of *n*-pentane. The entire solution was cooled to −30 °C for 1 week. Colorless cube-shaped crystals of the product were isolated by filtration. These crystals were dried under vacuum and characterized as $[(hfac)Ag]_4(SEt_2)$ by solution NMR, EA, and single-crystal X-ray diffraction. The characterization data are listed below.

Pd(hfac-*C*)(hfac-*O,O*)(SEt_2). IR (KBr disk, cm^{-1}): 2930 (vw), 1741 (m), 1670 (s), 1635 (m), 1610 (m), 1575 (w), 1560 (m), 1530 (s), 1490 (s), 1455 (m), 1339 (w), 1254 (s), 1203 (s), 1148 (s), 1178 (w), 1023 (w), 792 (s), 686 (m), 661 (m), 576 (m). NMR (C_7D_8): ^1H δ 5.94 (s, 1H, C*H* of hfac-*O,O*), 5.34 (s, 1H, C*H* of hfac-*C*), 1.97 (br m, 2H, SCH_2 of SEt_2), 1.57 (br m, 2H, SCH_2 of SEt_2), 0.82 (br t, 6H, J = 7.3 Hz, CH_3 of SEt_2); $^{13}C\{^1H\}$ δ 183.0 (q, $^2J(C-F)$ = 34.0 Hz, *C*=O of hfac), 117.4 (q, $^1J(C-F)$ = 285.6 Hz, CF_3 of hfac), 116.2 (q, $^1J(C-F)$ = 293.7 Hz, CF_3 of hfac), 91.6 (s, *C*H of hfac-*O,O*), 31.1 (s,

(5) Kodas, T. T.; Hampden-Smith, M. J. In *The Chemistry of Metal CVD*; Kodas, T. T., Hampden-Smith, M. J., Eds.; VCH: Weinheim, 1994; Chapter 9.
(6) Kaloyeros, A. E.; Feng, A.; Garhart, J.; Brooks, K. C.; Gosh, S. K.; Saxena, A. N.; Luethrs, F. *J. Electron. Mater.* **1990**, *19*, 271.
(7) Fannin, L. W.; Pearce, R. H.; Webb, D. W. *J. Electron. Mater.* **1994**, *23*, 93−96.
(8) Zheng, B.; Eisenbraun, E. T.; Liu, J.; Kaloyeros, A. E. *Appl. Phys. Lett.* **1992**, *61*, 2175−2177.
(9) Hansen, B. N.; Hybertson, B. M.; Barkley, R. M.; Sievers, R. E. *Chem. Mater.* **1992**, *4*, 749.
(10) Chen, S.; Mason, M. G.; Gysling, H. J.; Pazpujalt, G. R.; Blanton, T. N.; Castro, T.; Chen, K. M.; Fictorie, C. P.; Gladfelter, W. L.; Franciosi, A.; Cohen, P. I.; Evans, J. F. *J. Vac. Sci. Technol. A* **1993**, *11*, 2419−2429.
(11) Gysling, H. H.; Wernberg, A. A. *Chem. Mater.* **1992**, *4*, 900.
(12) Pike, R. D.; Cui, H.; Kershaw, R.; Dwight, K.; Wold, A.; Blanton, T. N.; Wernberg, A. A.; Gysling, H. J. *Thin Solid Films* **1993**, *224*, 221.
(13) Wernberg, A. A.; Gysling, H. J. *Chem. Mater.* **1993**, *5*, 1056.
(14) Wernberg, A. A.; Braunstein, G.; Pazpujalt, G.; Gysling, H. J.; Blanton, T. N. *Appl. Phys. Lett.* **1993**, *63*, 331−333.
(15) Wernberg, A. A.; Lawrence, D. J.; Gysling, H. J.; Filo, A. J.; Blanton, T. N. *J. Cryst. Growth* **1993**, *131*, 176−180.
(16) Wernberg, A. A.; Braunstein, G. H.; Gysling, H. J. *Appl. Phys. Lett.* **1993**, *63*, 2649−2651.
(17) Wernberg, A. A.; Gysling, H. J.; Braunstein, G. *J. Cryst. Growth* **1994**, *140*, 57−64.
(18) Weiss, F.; Frohlich, K.; Haase, R.; Labeau, M.; Selbmann, D.; Senateur, J. P.; Thomas, O. *J. Phys. IV* **1993**, *3*, 321−328.
(19) Deschanvres, J. L.; Bochu, B.; Joubert, J. C. *J. Phys. IV* **1993**, *3*, 485−491.
(20) Salazar, K. V.; Ott, K. C.; Dye, R. C.; Hubbard, K. M.; Peterson, E. J.; Coulter, J. Y.; Kodas, T. T. *Physica C* **1992**, *198*, 303−308.
(21) Valletregi, M.; Labeau, M.; Garcia, E.; Cabanas, M. V.; Gonzalez-calbet, J. M.; Delabouglise, G. *Physica C* **1991**, *180*, 57−60.
(22) Deschanvres, J. L.; Rey, P.; Delabouglise, G.; Labeau, M.; Joubert, J. C.; Peuzin, J. C. *Sensors and Actuators A−Physical* **1992**, *33*, 43−45.
(23) Deschanvres, J. L.; Bochu, B.; Joubert, J. C. *J. Phys. IV* **1993**, *3*, 485−491.
(24) Labeau, M.; Rey, P.; Deschanvres, J. L.; Joubert, J. C.; Delabouglise, G. *Thin Solid Films* **1992**, *213*, 94−98.
(25) Gautheron, B.; Labeau, M.; Delabouglise, G.; Schmatz, U. *Sensors and Actuators B−Chemical* **1993**, *16*, 357−362.
(26) Labeau, M.; Gautheron, B.; Delabouglise, G.; Pena, J.; Ragel, V.; Varela, A.; Roman, J.; Martinez, J.; Gonzalezcalbet, J. M.; Valletregi, M. *Sensors and Actuators B−Chemical* **1993**, *16*, 379−383.
(27) Deschanvres, J. L.; Joubert, J. C. *J. Phys. IV* **1992**, *2*, 29−33.
(28) Xu, C. Y.; Hampden-Smith, M. J.; Kodas, T. T. *Adv. Mater.* **1994**, *6*, 746−748.
(29) Roger, C.; Corbitt, T. S.; Hampden-Smith, M. J.; Kodas, T. T. *Appl. Phys. Lett.* **1994**, *65*, 1021−1023.
(30) Xu, C. Y.; Hampden-Smith, M. J.; Kodas, T. T. *Chem. Mater.* **1995**, *7*, 1539−1546.
(31) Shriver, D. F.; Dreyden, M. A. *The Manipulation of Air-Sensitive Compounds*, 2nd ed.; Wiley-Interscience: New York, 1986; p 78.
(32) Xu, C. Y.; Corbitt, T. S.; Hampden-Smith, M. J.; Kodas, T. T.; Duesler, E. N. *J. Chem. Soc. Dalton Trans.* **1994**, 2841−2849.

CH_2 of SEt_2), 30.8 (s, *C*H of hfac-*C*), 12.2 (s, *C*H_3 of SEt_2). Anal. Calcd for $C_{14}H_{12}PdF_{12}O_4S$: C, 27.54; H, 1.98. Found: C, 27.47; H, 1.87.

[(hfac)Ag]$_4$(SEt_2). IR (KBr disk, cm^{-1}): 2929 (vw), 1669 (s), 1650 (s), 1610 (m), 1530 (s), 1384 (w), 1490 (s), 1259 (s), 1203 (s), 1143 (s), 1078 (m), 792 (m), 661 (m), 581 (m). NMR (C_6D_6): ^1H δ 6.18 (s, 4H, C*H* of hfac), 1.67 (q, 4H, J = 7.5 Hz, SC*H*$_2$ of SEt_2), 0.64 (t, 6H, J = 7.5 Hz, C*H*$_3$ of SEt_2); $^{13}C\{^1H\}$ δ 177.8 (q, ^2J(C−F) = 31.5 Hz, *C*=O of hfac), 118.5 (q, ^1J(C−F) = 291.2 Hz, *C*F_3 of hfac), 87.1 (s *C*H of hfac), 28.2 (s, *C*H_2 of SEt_2), 14.6 (s, *C*H_3 of SEt_2). Anal. Calcd for $C_{24}H_{14}Ag_4F_{24}O_8S$: C, 21.35; H, 1.05. Found: C, 21.22; H, 1.09.

(b) Reaction between (hfac)Ag(SEt_2) and Pd(hfac)$_2$ in a 4:3 Mole Ratio. To examine the extent of this ligand exchange reaction in the correct (4:3) mole ratio, 50 mg (0.096 mmol) of Pd(hfac)$_2$ and 52 mg (0.128 mmol, 1.34 equiv) of (hfac)Ag(SEt_2) were mixed in 5 mL of dry benzene. The resulting solution was stirred for 1 h. Then 0.5 mL of this solution was transferred to an NMR tube. Removal of the solvent *in vacuo* in the NMR tube gave a yellow powder mixture. Then 0.5 mL of deuterated toluene was added to the tube. The ^1H NMR results showed the presence of Pd(hfac-*C*)(hfac-*O,O*)(SEt_2) and [(hfac)-Ag]$_4$(SEt_2), but only 45−50% of the Pd(hfac)$_2$ was converted to Pd-(hfac-*C*)(hfac-*O,O*)(SEt_2) according to integration.

To confirm this observation, ~5 mg of pure [(hfac)Ag]$_4$(SEt_2) and Pd(hfac)$_2$(SEt_2) were mixed and dissolved in toluene-d_8. The ^1H NMR spectrum clearly indicated the formation of Pd(hfac)$_2$. The chemical shift of the methine proton expected for hfac in [(hfac)Ag]$_4$(SEt_2) moved to slightly higher field.

(c) Independent Synthesis of Pd(hfac-*C*)(hfac-*O,O*)(SEt_2). A Schlenk flask was charged with Pd(hfac)$_2$ (2.00 g, 3.84 mmol); a stir bar and then 30 mL of toluene were added. The orange solid dissolved after stirring at 0 °C for several minutes; then diethyl sulfide (0.35 g, 3.88 mmol, 1.01 equiv) was added. The solution was stirred for 1 h, and a small amount of bright yellow crystalline product formed. The reaction mixture was concentrated by partial removal of the solvent *in vacuo* and was then cooled to −30 °C overnight. Removal of the solution by filtration gave 2.11 g (90% yield) of yellow, crystalline Pd(hfac-*C*)(hfac-*O,O*)(SEt_2), which gave satisfactory elemental analysis results. Anal. Calcd for $C_{14}H_{12}PdF_{12}O_4S$: C, 27.54; H, 1.98. Found: C, 27.42; H, 1.94. Mp: 132−132.5 °C. The IR and solution NMR data were exactly the same as those listed above. This product was sublimed intact at 75 °C and 10 mTorr.

(d) Independent Synthesis of [(hfac)Ag]$_4$(SEt_2). Silver(I) oxide (1.10 g, 4.75 mmol) was placed in a Schlenk flask (100 mL) wrapped with aluminum foil, and diethyl ether (15 mL) was added. The flask was cooled to 0 °C, and an aliquot of hfacH (2.10 g, 10.00 mmol, 1.06 equiv) was injected into the rapidly stirred solution by a syringe to form [(hfac)Ag]$_2$(H_2O). After 15 min, SEt_2 (0.23 g, 2.50 mmol, 0.25 equiv) was added by a syringe, and the entire solution was stirred at 0 °C for about 1 h and then cooled to −30 °C overnight. The reaction mixture was filtered to remove any insoluble components. The volatile components were removed *in vacuo* to give 3.00 g (93.6% yield) of crude crystalline product, which gave satisfactory elemental analysis results. Anal. Calcd for $C_{24}H_{14}Ag_4F_{24}O_8S$: C, 21.35; H, 1.05. Found: C, 21.05; H, 0.96. Mp: >151 °C dec. The IR and solution NMR data were exactly the same as those listed above.

X-ray Crystallographic Studies. A series of single-crystal X-ray diffraction studies of the solid-state structures of Pd(hfac-*C*)(hfac-*O,O*)-(SEt_2), [(hfac)Ag]$_4$(SEt_2), and (hfac)Ag(SEt_2) were carried out. A summary of the crystal data and experimental details for the X-ray diffraction studies of these compounds is presented in Table 1. A general description of the experimental procedure is presented here, with more details available as Supporting Information. The crystallographic data were obtained at 293 K with a 2θ range of 3.0−55.0° with ω scan type. In general, the structures were solved by either Patterson or direct methods. The non-hydrogen atoms were located through subsequent least-squares full-matrix cycles and difference Fourier calculations. Details of the refinement are given below for each individual structure. All software and the source of scattering factors are contained in the SHELXTL program library (G. Sheldrick, Nicolet Corp., Madison, WI).

Crystals of Pd(hfac-*C*)(hfac-*O,O*)(SEt_2) were grown from toluene at −30 °C, crystals of [(hfac)Ag]$_4$(SEt_2) were grown from ether/*n*-pentane (1:6, v/v) at −30 °C, and crystals of (hfac)Ag(SEt_2) were grown from *n*-pentane solution at −30 °C. Suitable crystals were selected and sealed in a glass capillary tube for (hfac)Ag(SEt_2) or attached to the tip of a glass fiber with grease for Pd(hfac-*C*)(hfac-*O,O*)(SEt_2) and [(hfac)Ag]$_4$(SEt_2).

Table 1. Summary of Crystal Data and X-ray Diffraction Experimental Details

	Pd(hfac-*C*)-(hfac-*O,O*)(SEt_2)	[(hfac)Ag]$_4$(SEt_2)	(hfac)Ag(SEt_2)
empirical formula	$C_{14}H_{12}PdF_{12}O_4S$	$C_{24}H_{14}Ag_4F_{24}O_8S$	$C_9H_{11}AgF_6O_2S$
fw	610.69	1349.87	405.12
color, habit	yellow prism	clear, colorless prism	colorless needle
unit-cell dimens			
a, Å	9.0273(9)	24.776(2)	10.853(4)
b, Å	26.248(3)	9.5179(8)	
c, Å	9.176(1)	19.940(3)	18.850(1)
β, deg	103.04 (1)	126.724(8)	
crystal system	monoclinic	monoclinic	hexagonal
space group	$P2_1/n$	$C2/c$	$P6_122$
T, K	293	293	296
λ, Å	0.710 73	0.710 73	0.710 73
Z	4	4	6
crystal size, mm	0.276 × 0.414 × 0.506	0.115 × 0.207 × 0.299	0.08 × 0.12 × 0.39
V, Å^3	2118.2(3)	3769.0(8)	1887(2)
no. of reflns collected	7916	6788	1396
no. of reflns used	2894	2384	482
abs coeff, mm^{-1}	1.097	2.266	1.836
$R(F)$,[a] %	6.73	5.23	9.36
$R_w(F)$,[b] %	7.54	5.15	10.49

[a] $R = \sum\Delta F/\sum F_o$. [b] $R_w = \sum w^{1/2}\Delta F/\sum w^{1/2}F_o$.

(a) Pd(hfac-*C*)(hfac-*O,O*)(SEt_2). The unit-cell parameters were obtained by the least-squares refinement of the angular settings of 46 reflections (4° < 2θ < 25°).

The systematic absences in the diffraction data are uniquely consistent for the space group $P2_1/n$. The structure was solved using the Patterson map interpretation, completed by subsequent difference Fourier synthesis and refined by full-matrix least-squares procedures. The trifluoromethyl groups exhibited positional disorder and were refined with idealized geometry. All non-hydrogen atoms were refined with anisotropic displacement coefficients except the disordered CF_3 groups which had idealized positions. Hydrogen atoms were treated as idealized contributions, except H(2) and H(7), which were located in the difference Fourier map. Atomic coordinates are presented in Table 2, and bond lengths and angles in Tables 5 and 6, respectively.

(b) [(hfac)Ag]$_4$(SEt_2). Refinement of all non-hydrogen atoms revealed residual electron density about C(10) and showed a total of three possible orientations for the F's on C(10). The three possible orientations for the F's on C(10) were included at equal occupancies (each set was set at $^1/_3$ occupancy). These positions were denoted as F(10), F(11), F(12); F(10′), F(11′), F(12′); and F(10″), F(11″), F(12″). The disordered atoms were refined isotropically. In the final refinement, all non-hydrogen atoms except disordered F's were treated anisotropically. Hydrogen atoms were included in idealized positions (riding model) with fixed isotropic U's set to 1.25U(eq) of the parent atoms. It is noteworthy that the crystal used changed from colorless to dark with concomitant reduction of 10% in the standard reflection intensities used to monitor the crystal integrity during data collection. Atomic coordinates are presented in Table 3, and bond lengths and angles in Tables 7 and 8, respectively.

(c) (hfac)Ag(SEt_2). Of the 1396 reflections collected, 829 were independent and 482 were observed [4$\sigma(F_o)$]. The structure was solved by direct methods. Refinement of the η parameter gave ambiguous results, and the true hand of the data could not be determined. Fluorine atoms were modeled as disordered idealized groups. The sulfur atom was located disordered in two independent positions, each position further disordered by a mirror plane. Ethyl groups on the thioether were not located but were included in the calculated parameters. Silver

Table 2. Atomic Coordinates ($\times 10^4$) and Equivalent Isotropic Displacement Coefficients (Å^2 $\times$ 10^3) for Pd(hfac-*C*)(hfac-*O*,*O*)(SEt_2)

	x	*y*	*z*	*U*(eq)[a]
Pd	1334(1)	1337(1)	3923(1)	47(1)
S	−25(3)	620(1)	4053(2)	48(1)
O(1)	−617(7)	1745(2)	3848(7)	60(2)
O(2)	2578(7)	1987(2)	3917(8)	64(2)
O(3)	2541(9)	154(3)	2598(8)	74(3)
O(4)	3377(8)	252(3)	5786(8)	75(3)
C(1)	−650(11)	2226(3)	3867(10)	55(3)
C(2)	544(12)	2565(3)	3958(11)	61(4)
C(3)	2010(11)	2423(3)	3976(10)	59(3)
C(4)	−2206(13)	2430(4)	3844(13)	74(4)
C(5)	3238(14)	2846(3)	4108(13)	77(4)
C(6)	3063(10)	579(3)	2674(10)	55(3)
C(7)	3354(10)	921(3)	4011(10)	52(3)
C(8)	3732(10)	673(3)	5480(11)	57(3)
C(9)	3454(13)	797(5)	1290(13)	77(4)
C(10)	4689(11)	978(4)	6733(13)	73(4)
C(11)	−1609(11)	651(4)	2441(11)	67(4)
C(12)	−1122(14)	581(4)	996(11)	80(4)
C(13)	−1009(11)	761(3)	5506(11)	60(3)
C(14)	98(14)	836(4)	7011(12)	82(5)
F(1)	−2214(17)	2802(6)	4778(18)	117(4)
F(2)	−3163(18)	2094(6)	4020(17)	108(4)
F(3)	−2771(17)	2655(6)	2470(17)	114(4)
F(1′)	−3237(21)	2218(7)	2674(21)	107(5)
F(2′)	−2407(20)	2904(7)	3614(21)	99(5)
F(3′)	−2762(21)	2255(7)	4919(22)	98(5)
F(4)	4228(14)	2799(4)	5407(14)	76(3)
F(5)	4066(16)	2782(5)	2982(14)	87(3)
F(6)	2722(14)	3302(5)	3832(15)	89(3)
F(4′)	3353(26)	2974(8)	2934(24)	114(6)
F(5′)	2637(16)	3293(5)	4642(17)	71(4)
F(6′)	4494(23)	2720(7)	4910(23)	91(6)
F(7)	3033(16)	496(5)	96(14)	108(4)
F(8)	2575(16)	1200(6)	789(15)	113(4)
F(9)	4834(18)	889(6)	1459(16)	117(4)
F(7′)	4493(35)	487(11)	857(32)	143(9)
F(8′)	2450(30)	844(11)	177(30)	127(8)
F(9′)	4476(26)	1188(9)	1525(23)	101(6)
F(10)	4071(16)	1419(5)	6913(16)	105(4)
F(11)	4999(15)	723(4)	8046(14)	101(3)
F(12)	6070(14)	1055(5)	6507(13)	103(3)
F(10′)	5821(28)	777(9)	7491(27)	114(7)
F(11′)	5431(26)	1416(8)	6237(24)	105(6)
F(12′)	3882(22)	1205(7)	7537(21)	86(5)

[a] Equivalent isotropic *U* defined as one-third of the trace of the orthogonalized $\mathbf{U}_{ij}$ tensor.

and oxygen atoms were refined anisotropically; hydrogen atoms were ignored; $R(F) = 9.36\%$, $R_w(F) = 10.49\%$. SHELXTL software was used for all computations (G. Sheldrick, Siemens XRD, Madison, WI). Absorption effects were compensated using the XABS program (H. Hope, UC-Davis, CA). Further details are available as Supporting Information. Atomic coordinates are presented in Table 4, and bond lengths and angles in Tables 9 and 10, respectively.

Results and Discussion

Toluene solutions of (hfac)Ag(SEt_2) and Pd(hfac)$_2$ mixed in various ratios have been used to deposit $Ag_{(1-x)}Pd_x$ films with various compositions by AACVD.[33] To determine whether or not these species reacted during the time scale of an AACVD experiment (approximately 15 min), they were mixed in a 1:1 mole ratio in toluene-d_8 and monitored by ^{1}H NMR spectroscopy. The ^{1}H NMR data revealed the presence of new resonances in the methine region of the β-diketonate and the methylene and methyl region of the ethyl sulfide ligand which could not be ascribed to either parent compound. To enable investigation of this reaction in more detail, (hfac)Ag(SEt_2) and Pd(hfac)$_2$ were mixed in a 1:1 mole ratio in toluene in a larger scale reaction from which two different crystalline fractions were obtained according to their different solubilities in toluene (see Experimental Section).

The first fraction obtained was characterized as Pd(hfac-*C*)(hfac-*O*,*O*)(SEt_2) according to combustion elemental analysis and NMR spectroscopy. The structure of this molecule was investigated in the solid state by a single-crystal X-ray diffraction study. An ORTEP plot is shown in Figure 1, and relevant bond lengths and angles are given in Tables 5 and 6. Like other Pd(hfac-*C*)(hfac-*O*,*O*)L compounds (e.g. L = $HN(CH_3)_2$, 2,6-

(33) Xu, C. Y.; Hampden-Smith, M. J.; Kodas, T. T. In *Mater. Res. Soc. Symp. Proc.* **1995**, *363*, 263−268.

Table 3. Atomic Coordinates ($\times 10^4$) and Equivalent Isotropic Displacement Coefficients (Å^2 $\times$ 10^3) for [(hfac)Ag]$_4$(SEt_2)

	x	*y*	*z*	*U*(eq)[a]
Ag(1)	2432(1)	1885(1)	5651(1)	52(1)
Ag(2)	799(1)	2733(1)	3870(1)	58(1)
O(1)	1280(3)	1794(7)	5147(4)	61(4)
O(2)	2433(3)	59(8)	6383(4)	63(4)
O(3)	1737(3)	1391(7)	4023(4)	46(3)
O(4)	3138(3)	798(6)	5212(4)	49(3)
C(1)	1089(5)	1394(11)	5577(6)	53(5)
C(2)	1421(5)	425(10)	6235(6)	54(6)
C(3)	2054(5)	−135(9)	6582(6)	48(5)
C(4)	430(6)	1989(15)	5332(9)	85(9)
C(5)	2328(7)	−1190(13)	7289(7)	69(8)
C(6)	1744(4)	158(10)	3805(5)	46(5)
C(7)	2293(4)	−734(10)	4136(5)	49(5)
C(8)	2958(5)	−305(10)	4799(6)	45(5)
C(9)	1055(5)	−395(12)	3099(7)	56(6)
C(10)	3532(6)	−1310(12)	5020(6)	71(7)
S	0	3807(4)	2500	55(2)
C(11)	492(9)	5044(17)	2382(9)	125(12)
C(12)	864(9)	4324(22)	2151(14)	167(20)
F(1)	−47(3)	1819(11)	4514(6)	129(6)
F(2)	175(4)	1450(11)	5673(6)	141(8)
F(3)	472(5)	3336(10)	5411(8)	166(11)
F(4)	2781(5)	−588(10)	8010(4)	143(7)
F(5)	2635(6)	−2218(9)	7251(5)	139(8)
F(6)	1905(4)	−1667(11)	7401(6)	156(8)
F(7)	736(3)	475(7)	2456(4)	88(4)
F(8)	676(3)	−520(7)	3363(4)	85(4)
F(9)	1056(3)	−1634(8)	2808(4)	104(5)
F(10)	3853(13)	−773(25)	4745(19)	76(6)
F(11)	3945(14)	−1478(29)	5859(14)	66(7)
F(12)	3319(9)	−2642(22)	4757(16)	44(5)
F(10′)	3581(13)	−1367(32)	4356(15)	85(6)
F(11′)	4097(11)	−1064(27)	5687(16)	76(7)
F(12′)	3370(15)	−2697(32)	5043(22)	99(13)
F(10″)	4089(9)	−563(19)	5269(16)	57(5)
F(11″)	3737(15)	−1888(30)	5805(18)	93(10)
F(12″)	3416(11)	−2201(29)	4504(15)	76(6)

[a] Equivalent isotropic *U* defined as one-third of the trace of the orthogonalized $\mathbf{U}_{ij}$ tensor.

Table 4. Atomic Coordinates ($\times 10^4$) and Equivalent Isotropic Displacement Coefficients (Å^2 $\times$ 10^3) for (hfac)Ag(SEt_2)

	x	*y*	*z*	*U*(eq)[a]
Ag(1)	954(2)	0	0	103(2)
O	−3(19)	1438(16)	293(7)	82(10)
C(1)	−2340(29)	0	0	70(10)
C(2)	−1230(25)	1209(25)	260(11)	61(7)
C(3)	−1314(1)	2547(1)	462(1)	162(16)
F(1)	−289	3382	909	123(11)
F(2)	−2552	2029	791	141(12)
F(3)	−1292	3283	−110	114(10)
F(1′)	−1389	2636	1169	113(10)
F(2′)	−2450	2473	161	176(16)
F(3′)	−164	3681	219	200(19)
S	2826(60)	−599(91)	266(41)	119(18)
S′	3354(36)	326(67)	195(29)	127(15)

[a] Equivalent isotropic *U* defined as one-third of the trace of the orthogonalized $\mathbf{U}_{ij}$ tensor.

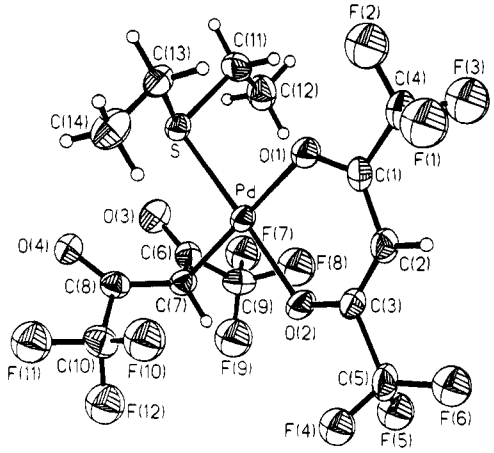

Figure 1. Molecular structure of $Pd(hfac)_2(SEt_2)$ in the solid-state as determined by single-crystal X-ray diffraction.

Table 5. Selected Bond Lengths (Å) for Pd(hfac-*C*)(hfac-*O,O*)(SEt_2)

Pd−S	2.264(2)	Pd−O(1)	2.050(6)
Pd−O(2)	2.044(6)	Pd−C(7)	2.111(9)
S−C(11)	1.812(9)	S−C(13)	1.799(11)
O(1)−C(1)	1.262(10)	O(2)−C(3)	1.260(11)
O(3)−C(6)	1.207(11)	O(4)−C(8)	1.201(12)
C(1)−C(2)	1.387(14)	C(1)−C(4)	1.500(15)
C(2)−C(3)	1.371(15)	C(3)−C(5)	1.555(14)
C(6)−C(9)	1.505(16)	C(6)−C(7)	1.494(12)
C(7)−C(8)	1.468(13)	C(8)−C(10)	1.504(13)
C(11)−C(12)	1.500(16)	C(13)−C(14)	1.524(13)

Table 6. Selected Bond Angles (deg) for Pd(hfac-*C*)(hfac-*O,O*)(SEt_2)

S−Pd−O(1)	88.0(2)	S−Pd−O(2)	177.2(2)
O(1)−Pd−O(2)	91.8(2)	S−Pd−C(7)	92.4(2)
O(1)−Pd−C(7)	179.5(2)	O(2)−Pd−C(7)	87.8(3)
Pd−S−C(11)	104.9(3)	Pd−S−C(13)	103.4(3)
C(11)−S−C(13)	99.5(5)	Pd−O(1)−C(1)	123.0(6)
Pd−O(2)−C(3)	121.9(6)	O(1)−C(1)−C(2)	128.5(9)
O(1)−C(1)−C(4)	112.5(8)	C(2)−C(1)−C(4)	118.9(8)
Pd−C(7)−C(8)	106.5(7)	C(6)−C(7)−C(8)	116.7(7)
O(4)−C(8)−C(7)	127.2(8)	O(4)−C(8)−C(10)	116.7(9)
C(7)−C(8)−C(10)	116.0(8)		

Me_2py, phenoxathiin, and phenazine),[34,35] this species is four-coordinate and square planar by virtue of the carbon-bonded nature of one of the hfac ligands. The solid-state structure indicates the hfac-*C* ligand has two uncoordinated carbonyl CF_3-CO groups. This is also reflected in the FTIR spectral data. In the solid-state FTIR spectrum of Pd(hfac-*C*)(hfac-*O,O*)(SEt_2), there is an absorption at 1741 cm^{-1} which is absent in the IR spectrum of $Pd(hfac)_2$, consistent with the presence of uncoordinated C=O groups in CF_3CO.

In solution, it appears that the integrity of this solid-state structure is retained as determined by ^1H NMR spectroscopy. At room temperature, two distinct hfac methine protons were observed at 5.94 and 5.34 ppm. The resonance at 5.94 ppm was assigned to the methine proton of the hfac-*O,O* ligand, and the resonance at 5.34 ppm was consistent with the methine proton of hfac-*C*, bonded to the sp^3 carbon, which was at rather low field since this sp^3 is carbon bonded to two electron-withdrawing groups. A similar assignment was reported previously for Pd(hfac-*C*)(hfac-*O,O*)L compounds, where L = $HN(CH_3)_2$, 2,6-Me_2py, phenoxathiin, and phenazine, where the methine proton at higher field was assigned to the methine proton of hfac-*C*, and confirmed by double-irradiation experiments.[35] The methyl protons of the ethyl groups occur as a broadened triplet while the methylene protons of the ethyl group occur as two broadened multiplets. Variable-temperature ^1H NMR spectroscopy showed that this broadening was the result of an exchange process where a broad multiplet was observed for the methylene protons at high temperatures and two distinct ABM_3 resonances were observed at lower temperatures as shown in Figure 2. The coalescence temperature was about 317 K with $\Delta\nu = 99.5$ Hz in the absence of exchange, giving an approximate activation barrier for exchange of $\Delta G^{\ddagger} \sim 14.8$ kcal/mol (61.9 kJ/mol). The inequivalence of the methylene protons at low temperatures and the retention of the two types of hfac methine resonances at high temperatures are consistent with an intramolecular exchange process which involves restricted rotation of the SEt_2 ligand about the S−Et bonds.

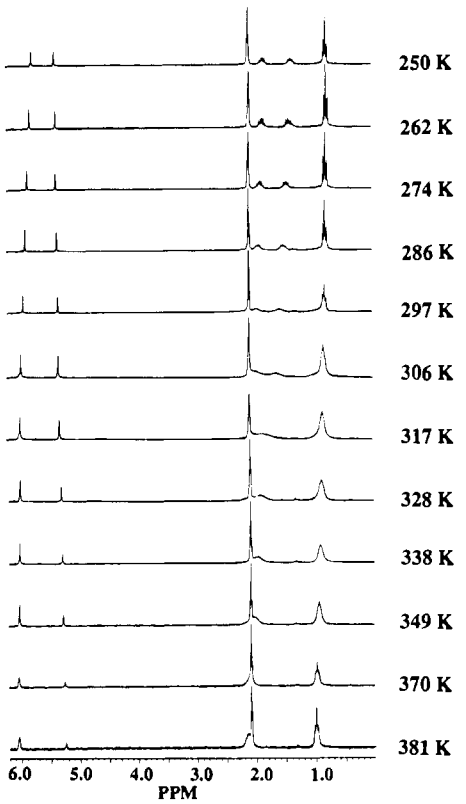

Figure 2. Variable-temperature ^1H NMR spectra of $Pd(hfac)_2(SEt_2)$ in toluene solution.

The $^{13}C\{^1H\}$ NMR spectrum showed two types of carbon resonances for the CF_3 groups, which is also consistent with the solid-state structural data and FTIR studies. There are two carbon resonances at 31.1 and 30.8 ppm which must be assigned to the hfac-*C* methine carbon or the methylene carbon of SEt_2. To distinguish these resonances, a $^{13}C\{^1H\}$ attached proton test (APT) NMR experiment was carried out. The results indicated the peak at 31.1 ppm is the signal of the methylene carbons in SEt_2 and the resonance at 30.8 ppm is the signal of the sp^3 methine carbon of the hfac-*C* ligand. This assignment is consistent with literature data where the carbon with $\delta = 29.5$ ppm and $J_{C-H} = 144$ Hz was assigned to the methine carbon of the hfac-*C* ligand in Pd(hfac-*C*)(hfac-*O,O*)(2,6-Me_2py).[35]

The other product of the reaction between (hfac)Ag(SEt_2) and $Pd(hfac)_2$ was also characterized in a fashion similar to that described above, which revealed the formation of $[(hfac)Ag]_4(SEt_2)$. Compared to the ^1H NMR spectrum of (hfac)Ag(SEt_2), the chemical shifts of the methylene and methyl protons in SEt_2 are shifted to slightly higher field. The $^{13}C\{^1H\}$ spectrum was almost the same as that of (hfac)Ag(SEt_2). According to the ^1H NMR spectra in deuterated benzene or toluene, only one type each of the hfac and SEt_2 ligands in $[(hfac)Ag]_4(SEt_2)$ was

(34) Siedle, A. R.; Newmark, R. A.; Pignolet, L. H. *Inorg. Chem.* **1983**, *22*, 2281−2286.
(35) Siedle, A. R.; Pignolet, L. H. *Inorg. Chem.* **1981**, *20*, 1849−1853.

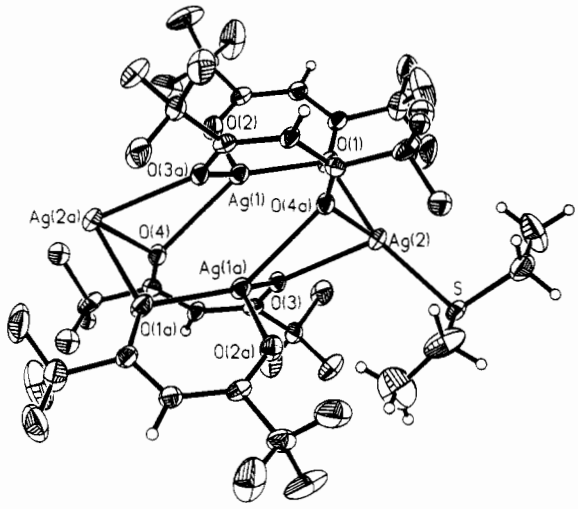

Figure 3. Molecular structure of $[(hfac)Ag]_4(SEt_2)$ in the solid state as determined by single-crystal X-ray diffraction.

Table 7. Selected Bond Lengths (Å) for $[(hfac)Ag]_4(SEt_2)$[a]

Ag(1)−O(1)	2.392(8)	Ag(1)−O(2)	2.268(9)
Ag(1)−O(4)	2.596(9)	Ag(1)−O(3a)	2.399(7)
Ag(2)−O(1)	2.251(7)	Ag(2)−O(3)	2.506(7)
Ag(2)−O(4a)	2.544(6)	Ag(2)−S	2.441(2)
O(1)−C(1)	1.263(17)	O(2)−C(3)	1.231(18)
O(3)−C(6)	1.256(12)	O(4)−C(8)	1.241(11)
C(1)−C(4)	1.507(20)	C(3)−C(5)	1.521(16)
C(1)−C(2)	1.399(13)	C(2)−C(3)	1.389(16)
C(6)−C(7)	1.390(14)	C(7)−C(8)	1.422(11)
C(6)−C(9)	1.517(11)	C(8)−C(10)	1.544(17)
Ag(1)- - -Ag(1A)	3.046(2)		

[a] Ag(1a), O(3a), O(4a) related to Ag(1), O(3), O(4) by the transformation $0.5 - x$, $0.5 - y$, $1 - z$.

observed. This is inconsistent with the expectation based on the retention of the solid-state structure in solution. There are two possible explanations for this observation: (i) $[(hfac)Ag]_4(SEt_2)$ dissociates to form a species with high symmetry in solution or (ii) the hfac and SEt_2 ligands undergo a rapid exchange process on the NMR time scale. A reaction to form a higher symmetry species is reasonable because most aromatic compounds can act as neutral donor ligands toward silver(I), such as in $(ClO_4)Ag(benzene)$, which results in deoligomerization of the polymeric species found in the solid state.[36-38]

$[(hfac)Ag]_4(SEt_2)$ was also characterized in the solid state by single-crystal X-ray diffraction, which revealed that this species exists as an infinite polymer with μ-SEt_2 groups, as shown in Figure 3. Metrical parameters for this species are presented in Tables 7 and 8. The structure of this species consists of discrete tetranuclear units bridged by a μ-SEt_2 group, resulting in the formation of infinite one-dimensional chains (see Figure 4). Each tetranuclear unit contains two types of hfac ligands: one exhibits a μ-η-O,η^2-O,O'-β-diketonate coordination mode, and the other exhibits a more unusual μ_4-β-diketonate coordination mode. The μ-η,η^2-coordination mode was observed previously in $\{[(hfac)Ag]_2NBD)\}_2$.[32] To our knowledge, this is the first time the μ_4-coordination mode has been observed for β-diketonate ligands. Also in the tetranuclear unit, there are two kinds of silver(I) atoms; one coordinates to the S atom of μ-SEt_2 and three O atoms from hfac, while the other coordinates only to the O atoms of hfac ligands. The Ag−O distances (from 2.251(7) to 2.596(9) Å) are similar to those observed in other $(hfac)ML_n$ (M = Ag, Cu) compounds. Unlike the case of other $(hfac)ML_n$ (M = Ag, Cu) compounds, in which the Lewis bases L ($L = XR_n$, X = O, S, P) usually acted as monodentate ligand,[32,39-41] in this compound, the SEt_2 ligand is monodentate and bridges the tetranuclear units to form a long chain polymer. The S−Ag bond length is 2.441(2) Å, slightly shorter than that of 2.468(2) Å observed in $(hfac)Ag(1,4\text{-thioxane})_2$ and similar (2.47(1) Å) to that found in $(hfac)Ag(SEt_2)$ (see below).[32] This μ-SEt_2 coordination mode is unusual. Two structures have been reported which also contain μ-SR_2 groups,[42,43] namely $[Pd_4(\mu\text{-}C_6H_4)_2(\mu\text{-}O_2CMe)_4(\mu\text{-S-}i\text{-}Pr_2)]$ and $[PPh_4][Cl_3W(\mu\text{-}SEt_2)(\mu\text{-}SEt)(\mu\text{-Cl})WCl_3]\cdot 2CH_2Cl_2$, but in both compounds the metals were also bridged by other ligands, μ-Cl in the case of the W≡W species and μ-C_6H_4 and μ-O_2CMe in the case of the Pd species. We believe that the structure of $[(hfac)Ag]_4(SEt_2)$ represents the first example of an unsupported μ-SEt_2 coordination mode.

Table 8. Selected Bond Angles (deg) for $[(hfac)Ag]_4(SEt_2)$[a]

O(1)−Ag(1)−O(2)	77.6(3)	O(1)−Ag(1)−O(4)	136.0(2)
O(4)−Ag(1)−O(2)	99.8(3)	O(1)−Ag(1)−O(3a)	138.9(2)
O(3a)−Ag(1)−O(2)	132.8(2)	O(4)−Ag(1)−O(3a)	73.8(2)
O(1)−Ag(2)−O(3)	80.5(3)	O(1)−Ag(2)−O(4a)	77.5(2)
O(3)−Ag(2)−O(4a)	73.0(2)	O(1)−Ag(2)−S	163.4(2)
O(3)−Ag(2)−S	115.0(2)	O(4a)−Ag(2)−S	111.9(2)
Ag(1)−O(1)Ag(2)	98.8(4)	Ag(1)−O(1)−C(1)	124.3(5)
Ag(2)−O(1)−C(1)	136.7(6)	Ag(1)−O(2)−C(3)	127.9(6)
Ag(2)−O(3)−C(6)	129.7(6)	Ag(2)−O(3)−Ag(1a)	105.5(2)
C(6)−O(3)−Ag(1a)	123.1(8)	Ag(1)−O(4)−C(8)	120.8(8)
Ag(1)−O(4)−Ag(2a)	98.9(2)	C(8)−O(4)−Ag(2a)	138.6(7)
O(1)−C(1)−C(2)	125.9(11)	O(1)−C(1)−C(4)	116.2(10)
C(2)−C(1)−C(4)	117.8(13)	C(1)−C(2)−C(3)	125.2(13)
O(2)−C(3)−C(2)	129.3(10)	O(2)−C(3)−C(5)	113.2(10)
C(2)−C(3)−C(5)	117.4(13)	O(3)−C(6)−C(7)	128.2(7)
O(3)−C(6)−C(9)	113.8(8)	C(7)−C(6)−C(9)	117.9(9)
C(6)−C(7)−C(8)	121.7(9)	O(4)−C(7)−C(8)	128.2(10)
O(4)−C(8)−C(10)	115.4(7)	C(7)−C(8)−C(10)	116.4(9)
Ag(2)−S−C(11)	105.0(4)	Ag(2)−S−Ag(2b)	130.5(2)

[a] Ag(1a), O(3a), O(4a) related to Ag(1), O(3), O(4) by the transformation $0.5 - x$, $0.5 - y$, $1 - z$. Ag(2b) related to Ag(2) by the transformation $-x$, y, $0.5 - z$.

As a result of the presence of this unusual coordination mode of the SEt_2 ligand, we decided to also determine the solid-state structure of the starting material $(hfac)Ag(SEt_2)$. We had previously assumed that the structure would be analogous to other (hfac)AgL compounds we had prepared previously, but the presence of the μ-SEt_2 coordination mode brought this assumption into question. The molecular structure of $(hfac)Ag(SEt_2)$ is shown in Figure 5, and the metrical parameters are presented in Tables 9 and 10. In the solid state, $(hfac)Ag(SEt_2)$ is monomeric with a chelating hfac ring and monodentate SEt_2, much like many other (hfac)ML compounds (M = Ag or Cu) that have been characterized previously.[39-41,44,45] However, the diffraction data are fairly poor and extensive discussion of these data is not warranted.

The observation of the ligand exchange reaction between $(hfac)Ag(SEt_2)$ and $Pd(hfac)_2$ mixed in a 1:1 mole ratio with formation of the species $Pd(hfac\text{-}C)(hfac\text{-}O,O)(SEt_2)$ and $[(hfac)Ag]_4(SEt_2)$ leads to the following balanced equation for the

(36) Gut, R.; Rueede, J. *J. Organomet. Chem.* **1977**, *128*, 89−93.
(37) Smith, H. G.; Rundle, R. E. *J. Am. Chem. Soc.* **1958**, *80*, 5074.
(38) Taylor, I. F. J.; Hall, E. A.; Amma, E. L. *J. Am. Chem. Soc.* **1969**, *91*, 5745.
(39) Shin, H.-K.; Hampden-Smith, M. J.; Kodas, T. T.; Duesler, E. N. *Can. J. Chem.* **1992**, *70*, 2954.
(40) Dryden, N. H.; Vittal, J. J.; Puddephatt, R. J. *Chem. Mater.* **1993**, *5*, 765.
(41) Lin, W.; Warren, T. H.; Nuzzo, R. G.; Girolami, G. S. *J. Am. Chem. Soc.* **1993**, *115*, 11644.
(42) Boorman, P. M.; Gao, X.; Parvez, M. *J. Chem. Soc., Dalton Trans.* **1992**, 25−31.
(43) Fuchita, Y.; Akiyama, M.; Arimoto, Y. *Inorg. Chim. Acta* **1993**, *205*, 185−190.
(44) Shin, H. K.; Chi, K. M.; Farkas, J.; Hampden-Smith, M. J.; Kodas, T. T.; Duesler, E. N. *Inorg. Chem.* **1992**, *31*, 424.
(45) Shin, H.-K.; Hampden-Smith, M. J.; Kodas, T. T.; Duesler, E. N. *Polyhedron* **1990**, *6*, 645.

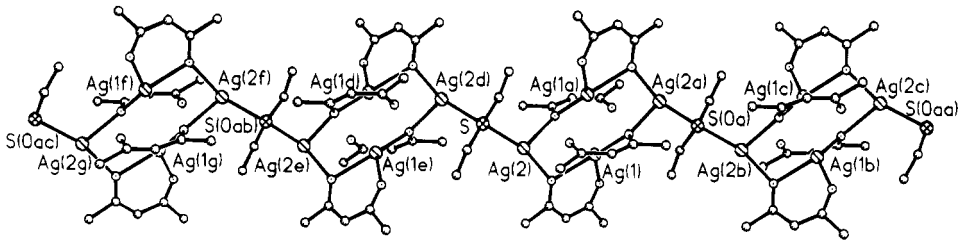

Figure 4. Crystal structure of $[(hfac)Ag]_4(SEt_2)$ shown by ball-and-stick drawing emphasizing the one-dimensional structure and the μ-SEt_2 coordination mode.

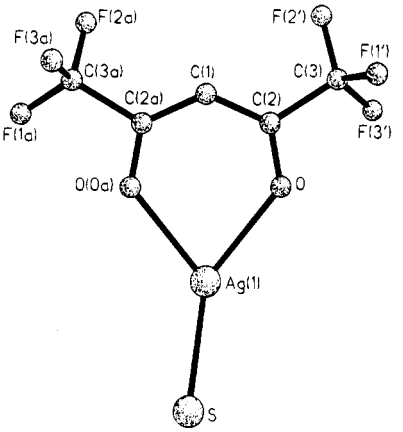

Figure 5. Molecular structure of $(hfac)Ag(SEt_2)$ in the solid state as determined by single-crystal X-ray diffraction.

Table 9. Selected Bond Lengths (Å) for $(hfac)Ag(SEt_2)$

Ag(1)−O	2.330 (23)	Ag(1)−S	2.473 (93)
Ag(1)−S′	2.473 (48)	Ag(1)- - -Ag(1a)	3.253 (2)
Ag(1)−O(Oa)	2.330 (17)		
O−C(2)	1.229 (35)		

Table 10. Selected Bond Angles (deg) for $(hfac)Ag(SEt_2)$

O−Ag(1)−S	146.1(18)	O−Ag(1)−S′	131.3(16)
O−Ag(1)−O(Oa)	77.4(9)	S−Ag(1)−O(Oa)	131.2(18)
Ag(1)−O−C(2)	130.9(15)	C(2)−C(1)−C(2a)	132.1(33)
O−C(2)−C(1)	124.4(28)	O−C(2)−C(3)	111.4(16)
C(1)−C(2)−C(3)	123.8(25)		111.8(9)

reaction:

$$4(hfac)Ag(SEt_2) + 3Pd(hfac)_2 \rightarrow 3Pd(hfac\text{-}C)(hfac\text{-}O,O)(SEt_2) + [(hfac)Ag]_4(SEt_2) \quad (1)$$

When this reaction was repeated by mixing the reagents in the correct mole ratios as defined by eq 1, the product Pd(hfac-*C*)(hfac-*O*,*O*)(SEt_2) was obtained in only 45−50% yield in solution, as determined by ^1H NMR integration, and unreacted $Pd(hfac)_2$ was observed. It is difficult to determine the relative amounts of $(hfac)Ag(SEt_2)$ and $[(hfac)Ag]_4(SEt_2)$ because it appears that these species undergo a ligand exchange process in solution. To further determine whether this reaction is reversible, pure Pd(hfac-*C*)(hfac-*O*,*O*)(SEt_2) and $[(hfac)Ag]_4(SEt_2)$ (i.e., the products of reaction 1) were mixed in toluene-d_8. The ^1H NMR spectrum obtained at room temperature showed the formation of $Pd(hfac)_2$ and the peaks associated with the presence of $(hfac)Ag(SEt_2)$ and $[(hfac)Ag]_4(SEt_2)$. The variable-temperature ^1H NMR spectra (Figure 6) are consistent with the existence of an equilibrium among all four species. At lower temperature, the less soluble Pd(hfac-*C*)(hfac-*O*,*O*)(SEt_2) crystallized out and displaced the equilibrium toward formation of $[(hfac)Ag]_4(SEt_2)$.

The ligand exchange reaction described above appears to occur as a result of the thermodynamic stability of the SEt_2 adduct, Pd(hfac-*C*)(hfac-*O*,*O*)(SEt_2). In order to prevent this ligand exchange reaction in solutions containing both Ag(I) and Pd(II) compounds required for AACVD of $Ag_{(1-x)}Pd_x$ alloys, it is reasonable to use Pd(hfac-*C*)(hfac-*O*,*O*)(SEt_2) as a Pd source. To determine whether Pd(hfac-*C*)(hfac-*O*,*O*)(SEt_2) and $(hfac)Ag(SEt_2)$ undergo ligand exchange (or any other reaction) in toluene solution, the two species were mixed in an equimolar ratio in toluene-d_8 and the integrity of the compounds was monitored by ^1H NMR spectroscopy. The ^1H NMR data revealed that these species do not react and so represent a suitable source of Ag and Pd reagents for the deposition of $Ag_{(1-x)}Pd_x$ alloys by AACVD. Studies of the AACVD of Ag/Pd alloy show that, under feed-rate-limited deposition conditions, high-purity films with controlled composition can be deposited.

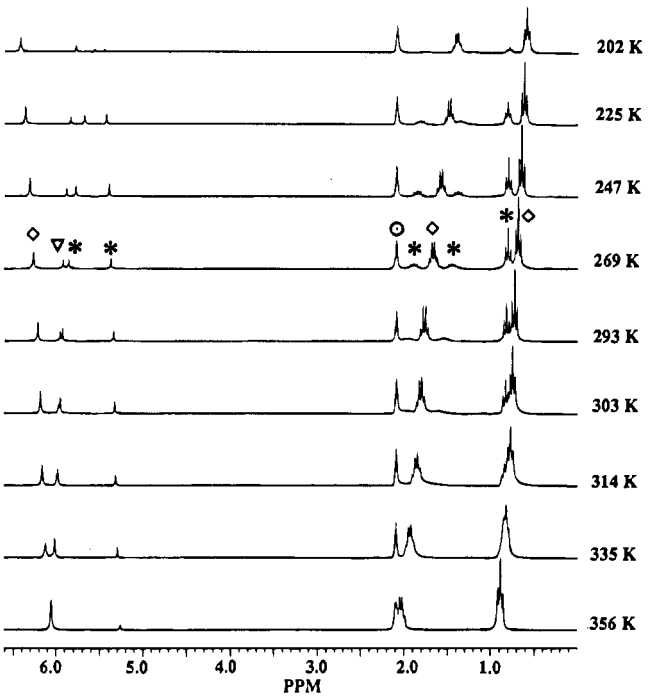

Figure 6. Variable-temperature ^1H NMR spectra of a mixture of $Pd(hfac)_2(SEt_2)$ and $[(hfac)Ag]_4(SEt_2)$ in toluene-d_8 confirming the reversibility of the reaction and emphasizing the equilibrium between all four components. At 269 K, the resonances have been labeled as follows for clarification: * = $Pd(hfac)_2(SEt_2)$; ▽ = $Pd(hfac)_2$; ◇ = $[(hfac)Ag]_4(SEt_2)$ and $(hfac)Ag(SEt_2)$; ⊙ = solvent.

Acknowledgment. M.J.H.-S. and T.T.K. thank the NSF (Grant CHE-9107035) for funding this work. M.J.H.-S. thanks the NSF Chemical Instrumentation Program for the purchase of a low-field NMR spectrometer and Nena Davis for technical assistance. C.X. thanks Dr. Todd Alam for assistance in obtaining the NMR spectra.

Supporting Information Available: Structure determination summaries and tables of bond lengths and angles, anisotropic displacement coefficients, and H atom coordinates (30 pages). Ordering information is given on any current masthead page.

IC9502133